Journal Name

ARTICLE

Impact of Oxygen Chemistry on Model Interstellar Grain Surfaces

A. Rosu-Finsen*,† and M. R. S. McCoustra

Received 00th January 20xx,
Accepted 00th January 20xx

DOI: 10.1039/x0xx00000x

www.rsc.org/

Temperature-programmed desorption (TPD) and reflection-absorption infrared spectroscopy (RAIRS) are used to probe the effect of atomic and molecular oxygen (O and O_2) beams on amorphous silica ($aSiO_2$) and water (H_2O) surfaces (porous-amorphous solid water; p-ASW, compact amorphous solid water; c-ASW, and crystalline solid water; CSW). Altering the deposition method of O_2 is shown to result in different desorption energies of O_2 due to differences in O_2 film morphology when deposited on the $aSiO_2$ surface. O_2 enthalpy of formation is dissipated into the $aSiO_2$ substrate without changes in the silica network. However, on the H_2O surfaces, O_2 formation enthalpy release is dissipated into the H-bonded matrix leading to morphological changes, possibly compacting p-ASW into c-ASW while CSW appears to undergo amorphisation. The enthalpy release from O_2 formation is, however, not enough to result in reactive desorption of O_2 or H_2O under the current experimental circumstances. Further to this, O_2 formation on sub-monolayer quantities of H_2O leads to enhanced de-wetting and a greater degree of H-bond reconnection in H_2O agglomerates. Lastly, O_3 is observed from the O + O_2 reaction on all surfaces studied.

Introduction

Oxygen is depleted from the gas phase in dense interstellar environments. This depletion is thought to be due to oxygen incorporation into interstellar dust grain materials[1] or into molecules on dust grains such as molecular oxygen (O_2) and ozone (O_3).[2] Therefore, laboratory studies of oxygen chemistry have been extensive. Direct desorption of O atoms has not been observed under laboratory UHV conditions, indicating that O atoms on interstellar surfaces convert fully[2] to O_2 and O_3 or are incorporated into other molecules such as water (H_2O), carbon monoxide (CO) and methanol (CH_3OH). Molecules such as O_3, H_2O, CO and CH_3OH are infrared active and so their contribution to the known sinks for oxygen can be evaluated. The same cannot be said for O_2 with its low IR activity. However, thermal desorption experiments on O_2 have inferred a solid state lifetime on interstellar dust grains of around 10^9 years.[3] The formation of O_2 and O_3 along with such molecules being frozen out on interstellar dust grain surfaces, and not returned to the gas-phase through changes in surface temperature, could explain part of the oxygen abundance controversy.

H_2O is the most abundant molecule in the solid mantles coating interstellar dust grains. Consequently, H_2O formation has been extensively studied. The main formation pathway of H_2O is through hydrogenation reactions of O, O_2, and O_3 in the solid state on interstellar surfaces[4-7] leading to, what is believed to be mainly, compact amorphous solid water (c-ASW).[8] Upon formation on grain surfaces, or upon adsorption from the gas phase, H_2O has been shown to be free to agglomerate into clusters.[9] Diffusion of atoms in search of a reaction partner on interstellar surfaces is not a new concept.[10,11] Likewise, molecular diffusion, *e.g.* of CO, has been inferred from monolayer formation on both SiO_2 and H_2O surfaces[3,12,13] and from observations of the line shapes of the C=O stretching vibration.[14] However, the mobility, or otherwise, of H_2O has received little attention as the stick-and-stop assumption of ballistic accretion is normally applied. However, the observation that H_2O always desorbs with multilayer kinetics prompted a detailed IR investigation of the thermal behaviour of H_2O. This work concluded that H_2O prefers to form three dimensional agglomerates as opposed to a two-dimensional monolayer at strikingly low laboratory temperatures.[9] This, in turn, suggested a revision of the onion model of icy interstellar grain mantles.

As time progresses, formation of other interstellar ice components can therefore occur on H_2O or $aSiO_2$ surfaces. Just as $aSiO_2$ acts as an energy sink in H_2O formation, so too can H_2O act as an energy sink for molecule-forming reactions by dissipating energy into its hydrogen-bonded matrix. Such input and dissipation of energy can lead to morphological changes. Indeed, morphological changes of H_2O films have been shown during D atom,[15] electron[16,17] and photon[18] bombardment of H_2O. Additionally, changing the deposition method of H_2O also leads to structural differences.[19,20]

This paper is structured in such a way as to highlight experimental observations made during a study of O + O reactivity on $aSiO_2$ surfaces and on H_2O ice (porous amorphous solid water, p-ASW; compact amorphous solid water, c-ASW; and crystalline solid water, CSW) surfaces. The conclusions

Institute of Chemical Sciences, Heriot-Watt University, Riccarton, Edinburgh, EH14 4AS, United Kingdom
**Corresponding author: a.rosu-finsen@ucl.ac.uk*
† Present Address: Department of Chemistry, University College London, 20 Gordon Street, London, WC1H 0AJ, United Kingdom

with respect to the formation of O_2 and O_3 from these studies are similar to those existing in the literature and not reported here in detail other than to report on desorption of O_3 as formed through oxygen chemistry on $aSiO_2$ and water surfaces. However, our observations on the impact of dosing and reactivity on the morphology of both solid O_2 and H_2O ices are novel and point to the key role for reaction enthalpy release in this system.

Experimental

A general description of the experimental apparatus employed in this work has been given previously.[21,22] However, the present experiments warrant repetition in a brief manner. All experiments were conducted in a 30 cm diameter UHV chamber capable of reaching a base pressure of about 1×10^{-10} mbar. A copper sample block coated with 300 nm of amorphous silica ($aSiO_2$) is located in the chamber and connected to a closed-cycle He cryostat (APD Cryogenics, HC-2) which can cool the sample to 17 K as measured by a KP-type thermocouple. A cartridge heater (Heatwave Labs Inc., TB–175) is situated inside the sample block to ensure uniform heating of the sample surface as required for temperature-programmed desorption (TPD) experiments. Two differentially-pumped, radio frequency (RF) plasma sources are attached to the main UHV chamber of which only the O_2 source is used in this work. The plasma source is capable of dissociating O_2 to O (ground state, O ^{3}P) with an efficiency of about 20%. The flux from the source is estimated to be $(5.8 \pm 0.4) \times 10^{14}$ molecules cm^{-2} s^{-1} at the cold substrate. Thin films equivalent to 5 monolayers (ML) of O_2 were deposited using the plasma source with the RF power turned off for pure O_2 or with the RF power on to produce a mixed O:O_2 beam. A ML coverage was defined through TPD experiments showing the sub-monolayer to multilayer transition through increasing dosing time akin to background dosing experiments reported by Collings *et al.*[3] These experiments are not shown, however, 10 minute O_2 beam dosing produces 1 ML.

Also attached to the chamber is an FTIR spectrometer (Varian 670-IR) optically configured for reflection-absorption infrared spectroscopy (RAIRS) with a grazing incidence angle of 75° to the surface normal. For such measurements, 512 scans were co-added to form each spectrum and recorded with a 1 cm^{-1} resolution. A line-of-sight quadrupole mass spectrometer (QMS, Hiden analytical Ltd., HAL301) is used for the TPD experiments with heating rates of 0.24 K s^{-1} and 0.17 K s^{-1} for the O_2 and O_3 experiments, respectively.

Results and Discussion

Growth and Desorption of O_2 Films

O_2 formation and desorption have been examined previously.[3,22-25] However, in this work we intend to add insight by comparing O_2 desorption following three different deposition methods. Fig. 1 shows the O_2 desorption from $aSiO_2$ when normalised to the individual TPD profile maximum QMS count rate. The red trace is for O_2 as produced from O:O_2 beam deposition, pure O_2 molecular beam dosing is in blue and, lastly, background dosing as taken from Collings *et al.*[3] in black. All three traces can be seen to share a similar leading edge of desorption starting at about 26 K, however, beyond 27 K changes in the behaviour are observed resulting in desorption traces with significantly different profiles. Molecular beam deposited O_2 leads to TPD data with a peak desorption temperature of about 29.5 K while the two other traces are about 1 K higher. During the various experiments, O atoms (m/z = 16) were monitored with the QMS. However, at no point were there any signs of direct O atom desorption observed, outside of the expected cracking pattern of O_2 and O_3 for our QMS operating conditions. This indicates that all O atoms on the $aSiO_2$ surface were consumed in the O_2 and O_3 formation reactions. Also, reactive desorption of O_2 during O atomic beam deposition was not observed indicating that there is insufficient energy present to overcome the O_2 desorption barrier.

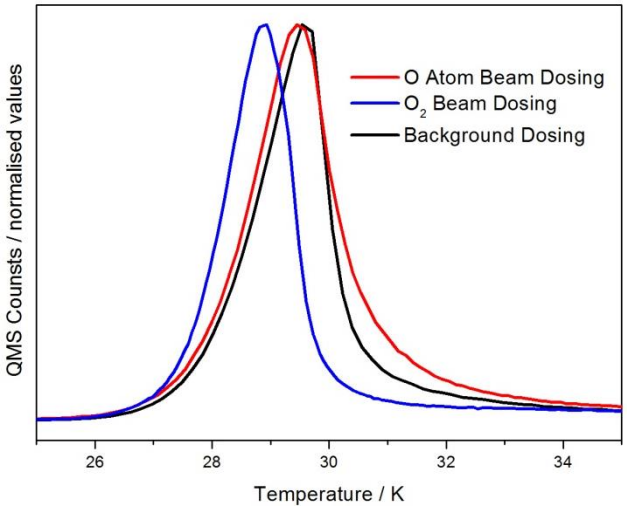

Fig. 1: This figure shows the comparison of O_2 desorption from $aSiO_2$. The blue trace is of molecular beam dosed O_2, while red is atomic beam dosed O_2. The black trace is taken from Collings *et al.* **[3]** for comparison and is of background dosed O_2. All experiments are of 5 ML O_2 films and have been normalised to each trace's respective maximum QMS count to highlight differences in equivalent molecular systems when deposition methods are varied.

The experimental data were modelled as previously described in Collings *et al.*[3] Plotting the experimental rate of desorption (v_{des}) from Fig. 1 in an Arrhenius manner and assuming zero order kinetics as consistent with multilayer desorption,

$$v_{des} = k, \qquad \text{Equation 1}$$

we obtain Equation 2:

$$ln(k) = ln(\nu) - \frac{E_{des}}{RT}. \qquad \text{Equation 2}$$

Here, k is the rate constant for the desorption process, ν is the pre-exponential factor, E_{des} is the activation energy for desorption, R is the ideal gas constant and T is the absolute temperature. Fitting the leading edge of the desorption profile with a straight-line yields a first approximation to the activation energy for desorption and pre-exponential factor which can be refined to obtain the kinetic parameters for desorption in this molecular system.

O_2 Deposition Method	E_{des} / kJ mol^{-1}	ν / molecules cm^{-2} s^{-1}
O_2 beam on $aSiO_2$	8.5 ± 0.1	$4 \times 10^{30\pm1}$
O_2 reactive accretion on $aSiO_2$	6.7 ± 0.1	$5 \times 10^{27\pm1}$
O_2 reactive accretion on p-ASW	7.4 ± 0.6	$1 \times 10^{25\pm2}$
O_2 reactive accretion on c-ASW	6.3 ± 0.4	$1 \times 10^{26\pm2}$
O_2 Reactive accretion on CSW	6.7 ± 0.2	$5 \times 10^{27\pm1}$
O_2 Background Dosed[3]	7.5 ± 0.2	$1 \times 10^{28\pm1}$

Table 1: This table lists the data gathered from the TPD experiments of O_2. All experiments are of 5 ML O_2 films deposited by the stated methods and desorbed from the specified surface. The final row is of O_2 background dosed onto $aSiO_2$ as found in the literature.[3]

Table 1 reports the best-fit parameters derived from the refinement. Interestingly, different desorption energies are observed of the same molecular system and same 5 ML molecular film thickness depending on the method of film preparation. This type of behaviour has previously been reported in H_2O by Kimmel *et al*.[19,20] and associated with differences in film morphology.

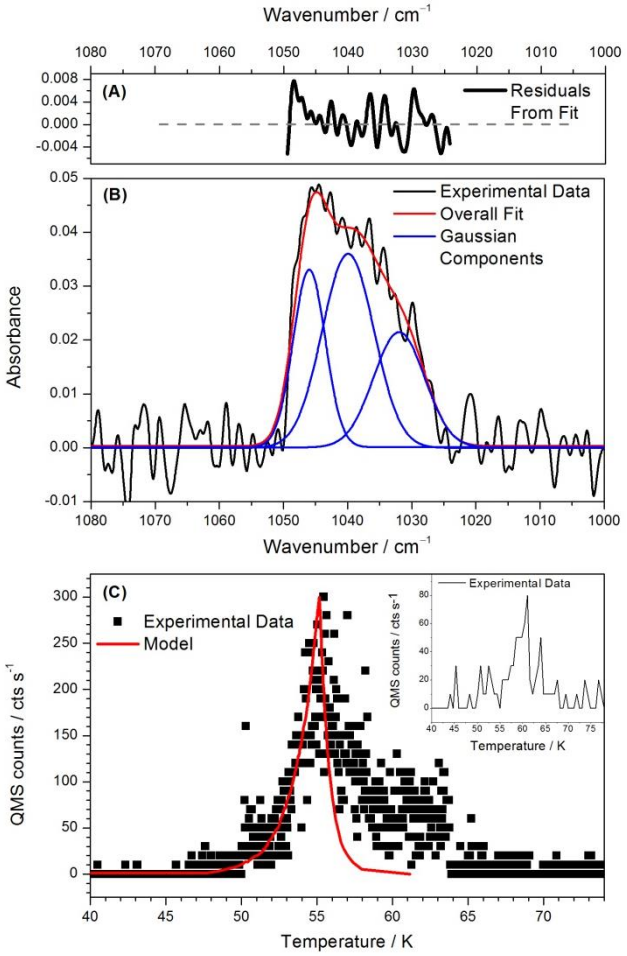

Fig. 2: This figure is comprised of three panels of which the upper two relate to RAIRS experiments observing the O_3 feature. The experimental data in Panel (B) is shown in the solid black line with a fit of the band shown in red and comprises of three Gaussians marked in blue. Panel (A) is of the residuals between the experimental data and the fit. The bottom panel, (C), is of the TPD experiment showing experimental data as black squares and a model in red. The assignment of the RAIR spectrum is given in **Table 2**.

Background dosing results in a slower rate of molecular deposition compared to beam dosing and an open film structure as energy release is fully accommodated in individual adsorption events. In contrast, beam dosing generally results in the formation of a more compact film as some energy accumulation can occur in the film resulting in annealing during accommodation. The more open the film structure, the lower the corresponding E_{des} as the average coordination number of species in the film is reduced.

Such behaviour is also possible for O_2 and our data confirm this. Comparing the O_2 beam dosing to O_2 background dosing, Table 1 lists the E_{des} as 8.5 ± 0.1 and 7.5 ± 0.2 kJ mol^{-1}, respectively. The pre-exponential factors also support this view. For the compact O_2 beam generated film, ν, takes the value of $4 \times 10^{30\pm1}$ molecule cm^{-2} s^{-1}, while that of the open background dosed film is $1 \times 10^{28\pm1}$ molecule cm^{-2} s^{-1}. The pre-exponential factors within a Transition State Theory framework are exponentially linked to the activation entropy for desorption, $\Delta^{\ddagger}S_{des}$. It is likely that a compact, more ordered film would see a larger change in entropy in forming the transition state for desorption than in the situation where the film is open and the coordination of surface species already reduced. A larger activation entropy in turn would mean a larger pre-exponential as we observe.

Let us now consider the case of the O_2 film prepared by reactive accretion from the O:O_2 beam. Comparison of the TPD data in Figure 1 suggests that the resulting film is more consistent with the film morphology when O_2 is background dosed; *i.e.* open and disordered. The analysis of the TPD data reinforces this with E_{des} and ν, 6.7 ± 0.1 kJ mol^{-1} and $5 \times 10^{27\pm1}$ molecule cm^{-2} s^{-1} respectively, being more consistent with the equivalent parameters from the open, more fragmented, structure of the background dosed O_2. This would clearly indicate that reaction enthalpy release is not dissipated into compaction by annealing of the product O_2 solid. Nor, as we reported above, did we observe O_2 desorption. Our only conclusion therefore is that the reaction enthalpy is efficiently channelled into the growing O_2 films as well as into the $aSiO_2$ substrate; probably as a result of a strong interaction between the O_2 monolayer and the substrate.

O_3 Formation and Thermal Desorption

Fig. 2 summarises the RAIRS and TPD measurements on the formation of O_3 *via* the surface O + O_2 reaction as reported in the thesis of Rosu-Finsen.[26] Fig. 2(b) shows the O_3 RAIR feature (black line), where the principal mode is the O_3 asymmetric stretch, that appears as O_3 is synthesised from the O + O_2 reaction on $aSiO_2$. Other O_3 vibrational modes (the O–O symmetric stretch or the O–O–O bending mode) were not detected in this work due to overlapping of gas phase water feature from the purged external optics. The line is broad and displays evidence of three components consistent with O_3 in three different environments as proposed by Kaiser and co-workers: [O_3…O], O_3 asymmetric stretch and [O_3…O_3].[27] Such environmental sensitivity is a well-established feature of vibrational spectroscopy in the solid state and on surfaces. Indeed, as we have recently demonstrated in relation to the environmental sensitivity of the IR spectroscopy of CO on astronomically relevant solid surfaces.[14] A three component

Assignment	Wavenumber / cm^{-1}	
	This work	Literature[27]
[O_3…O]	1031 ± 1	1032 ± 2
O_3 (O–O) asym. stretch	1036 ± 1	1037 ± 2
[O_3…O_3]	1045 ± 1	1042 ± 2

Table 2: This table lists the result of the Gaussian fits in terms of the positions of individual contributions making up the overall O_3 feature in **Figure 1(b)**. The final column compares the experimentally obtained wavenumber values to the literature.[27]

Gaussian fit (fit in red and components in blue) clearly reproduces the experimental data. The upper panel, Fig. 2(a), shows the residuals of the fitting procedure with the light-grey line indicating a zero value for the residual. The peak positions of each blue Gaussian component are listed in Table 2 with a comparison with existing literature values.[27]

Fig. 2(c) compares the experimental TPD data (black squares) to a modelled fit (red solid line). Desorption of O_3 has been noted in the literature from a variety of sources.[2,28-30] Formation of O_3 through O + O_2 and subsequent desorption typically shows that O_3 starts to desorb from ≥ 55 K. O_3 monolayer desorption peaks at about 60 K and upwards depending on molecular coverage.[2] In the present work, direct detection of O_3 through m/z = 48 was difficult, yielding minimal experimental data. Indeed, m/z = 48 is a 20% mass fragment of O_3 when analysed by mass spectrometry while m/z = 32 is the dominant mass fragment.[31] However, as the sample temperature increases to > 50 K cold finger desorption of O_2 from the He cryostat occurs. Distinguishing between O_3 desorption from the sample and O_2 desorption from the cold finger becomes impossible leading to m/z = 48 as being the detection method of gas-phase O_3. The insert in Fig. 2 (c) shows the raw data of O_3 desorption from a single experiment as monitored through the m/z = 48 mass channel. Summation of all experimental results of O_3 desorption leads to the trace in black squares presented in Fig. 2 (c). The heating rate being equivalent for O_3 desorption throughout all experiments lead to a straight-forward summation of the data to produce the TPD trace. The predominant reason for only detecting a slight amount of O_3 is believed to be due to O_3 dissociation in the head of the mass spectrometer source. O + O_3 is also a possible reason leading to decreased O_3 abundance. However, Minissale *et al.*[2] reason this destruction as being negligible due to a reaction barrier as earlier argued by Atkinson *et al.*[32]. The trace presented in Fig. 2 (c) peaks at about 55 K which we note as being earlier than literature values, however, this may be due to the addition process. Trailing edges in thin film TPD experiments have previously been ascribed to a lower molecular level of exposure, *i.e.* mono- or sub-monolayer coverage.[3] However, the separate monolayer desorption peak as noted by Minissale *et al.*[2] was not observed in this work. Due to the relative amount of O_3 detected and the co-addition process resulting in Fig. 2(c) we conclude that the O_3 TPD spectrum presented is less resolved than desired.

Analysis of the TPD spectrum according to the method outlined above yields 14.7 ± 0.5 kJ mol^{-1} for the activation energy for desorption, which compare well to literature values of 15.2 ± 0.5 kJ mol^{-1},[28,30] and a pre-exponential factor of $1 \times 10^{28\pm2}$ molecules cm^{-2} s^{-1}. However, due to the addition process needed to produce the O_3 TPD trace, the uncertainty related to our 14.7 kJ mol^{-1} may, in fact, be greater.

Impact of the O + O Reaction on Solid H_2O Deposits

Previous work has demonstrated that H_2O has a propensity to de-wet on $aSiO_2$ and HOPG surfaces at temperatures as low as 17 K and 24 K, respectively.[9] The rate constant associated with the de–wetting process at 17 K is comparatively low (2.5×10^{-5} s^{-1}) and full de-wetting at 17 K takes place on a timescale longer than the experiments in the O + O investigations that form the basis of this paper. This allows us to investigate the impact of enthalpy release from the formation of O_2 on potentially very small quantities of H_2O ballistically deposited on our $aSiO_2$ substrate.

Fig. 3 reports the time evolution of the intensity of the OH stretching vibration (vOH) of 0.5 ML equivalent of H_2O on $aSiO_2$ as it is bombarded with O atoms from the O:O_2 beam. The data show the same general trend as in our previous studies of H_2O de-wetting from $aSiO_2$;[9] the intensity of the main band centred at about 3250 cm^{-1} increases with time and atomic O bombardment. As we are not adding H_2O to the surface, the intensity increase can, as in reference [9], only be associated with an increase in the degree of hydrogen bonding within the adlayer. This could be due to either enhanced H_2O agglomeration and / or increased hydrogen bond connectivity within H_2O agglomerates, *i.e.* conversion of p-ASW to c-ASW.

Rate constants for the O atom-induced vOH band intensification process have been determined as previously assuming first order kinetics:[33]

$$ln\left(\frac{A_\infty - A_0}{A_\infty - A_t}\right) = kt \qquad \text{Equation 3}$$

where A_∞ is the area of the vOH band of the final vOH spectrum after 50 minute O atom bombardment, A_0 is the area of the initial H_2O vOH spectrum before O atom irradiation and A_t is the area of the vOH after the specified O atom bombardment time. The rate

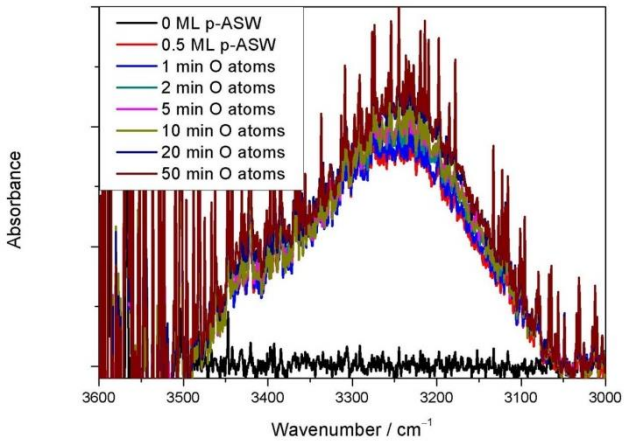

Fig. 3: This figure shows the OH stretching region of the RAIR spectrum of 0.5 ML p-ASW deposited on $aSiO_2$ and bombarded with O atoms for the times specified in the legend. The sharp features clearly visible in the spectrum associated with the 50 min O atom irradiation are due to gas-phase H_2O contamination in the optics boxes external to the UHV chamber.

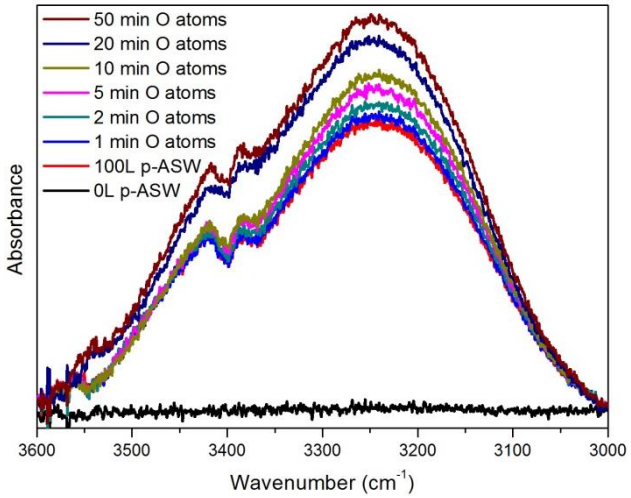

Fig. 4: This figure shows the OH stretching region of the RAIR spectrum of 1.0 ML p-ASW deposited on $aSiO_2$ and bombarded with O atoms for the times specified in the legend.

constant, *k*, for the de-wetting process is calculated to be (1.8 ± 0.2) × 10^{-3} s^{-1}. This value is about 2 orders of magnitude larger than for the same process occurring isothermally on $aSiO_2$ in the absence of O atom bombardment as mentioned previously.[9] Hence O atom bombardment appears to enhance the rate of H_2O agglomeration on the $aSiO_2$ surface.

Fig. 4 shows what happens when a 1.0 ML p-ASW film is irradiated with O atoms. Again, an increase in the general intensity of the vOH band is observed with O atom irradiation time. In this instance, the rate constant for the de-wetting process is calculated to be (1.2 ± 0.2) × 10^{-3} s^{-1} consistent with the previous measurement.

While there is a noticeable amount of noise in the spectra in Fig. 3, less so in Fig. 4, the vOH band is observed to be asymmetric with a shoulder at about 3400 cm^{-1}. This region of the vOH band and at higher wavenumbers has previously been ascribed to smaller

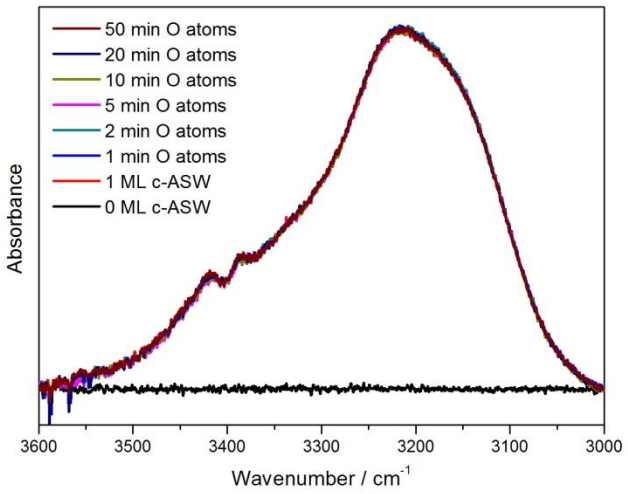

Fig. 5: This figure shows the OH stretching region of the RAIR spectrum of 1 ML of c-ASW on $aSiO_2$ following irradiation by O atoms for the times specified in the legend. No changes are observed as time and O atom bombardment progress.

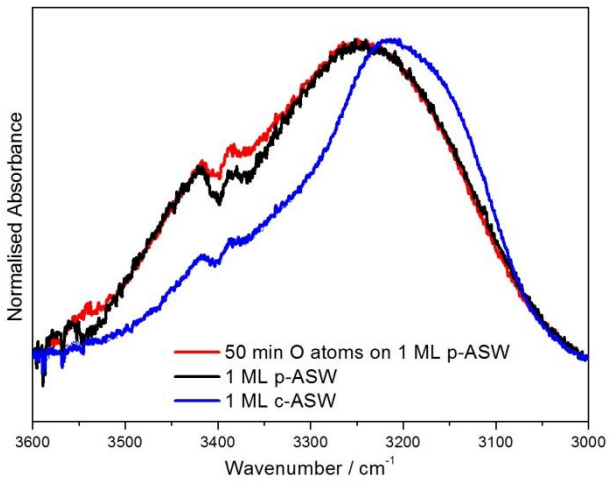

Fig. 6: This figure shows the comparison of the normalised H_2O spectra as labelled in the legend. Each spectrum has been normalised to its maximum peak absorbance.

clusters of H_2O.[34,35] Clear changes can be seen in this region in Fig. 4 with O atom dosing, which could relate to hydrogen-bond network reconnection by morphological changes or hydrogen-bond network extension by enhanced agglomeration. Morphological changes in p-ASW thin films (≤ 8 ML) have been shown to occur upon bombardment with a D atomic beam.[15] However, considering the low number-density of H_2O on the $aSiO_2$ surface in the present work, and the rough nature of the $aSiO_2$ surface,[36] hydrogen-bond network extension by agglomeration is the more likely process promoting changes in shape and intensity of the vOH band.

Thus, as O atoms are deposited and are free to diffuse on either surface,[11] O_2, likely, initially forms on either surface. The absence of product O_2 desorption then suggests that the reaction enthalpy is dissipated into the substrate promoting hydrogen-bond network extension by agglomeration and, hence, the changes observed in the high-wavenumber regime of the vOH band.

Changing the morphology of the underlying H_2O layer from p-ASW to c-ASW confirms this speculation. Fig. 5 shows the impact of O atom irradiation on 1 ML of c-ASW (*i.e.* amorphous solid water in which the hydrogen-bond network is fully connected). There is no vOH band intensity increase as time and O atom bombardment progress. This is simply a consequence of both hydrogen-bond network extension by agglomeration and hydrogen-bond network reconnection by morphological change having been completed at the higher deposition temperature (100 K) used to grow the c-ASW film. Thus, c-ASW is unaffected by the reaction enthalpy release in forming O_2.

Fig. 6 shows the comparison of the vOH band for 1 ML of p-ASW in black with the same film after 50 minute O atom irradiation (red line). The vOH band of 1 ML c-ASW film is also shown in blue. The spectra have been normalised to their respective maximum intensities to show differences between the vOH band of p-ASW, before and after O atom irradiation, and of c-ASW. Only the initial 1 ML p-ASW and 50 minute O atom spectra are shown to focus on band differences over irradiation time. As c-ASW films appear to be invariant with O atom irradiation (Fig. 5), the 1 ML coverage was

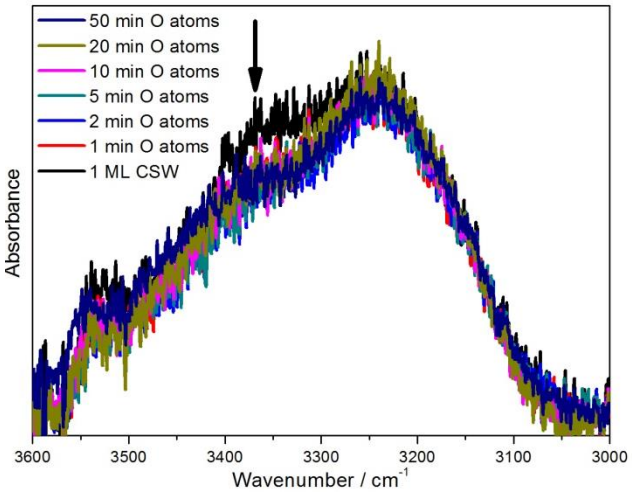

Fig. 7: The RAIR spectra in the OH stretching region of 1 ML CSW on $aSiO_2$ under bombardment with O atoms. Note the disappearance of the shoulder indicated with the arrow after O atom bombardment.

chosen as a comparison. The c-ASW νOH band is shifted towards lower wavenumber. Features in the 3400 cm^{-1} range appear in all spectra and are invariant in position. The relative intensities of the 3380 cm^{-1} features are also invariant between the systems. However, the features at about 3420 cm^{-1} and 3550 cm^{-1} do exhibit variation between the systems. The 3420 cm^{-1} feature exhibits a clear change in the size of the peak on the high-wavenumber trailing edge of the νOH band. While, in the 3550 cm^{-1} feature, the c-ASW and 50 minute O atom spectra are comparable while distinct from the p-ASW trace. Clearly, excess energy from O_2 formation dissipated into the p-ASW leads to qualitative changes in the spectra transforming the features observed on the νOH band of p-ASW into features more consistent with c-ASW with 50 minutes of O atom irradiation.

One final question to address is what happens to a CSW film with O atom irradiation. Fig. 7 shows the result of O atom bombardment of a CSW film in black. Our initial 1 ML CSW film shows a shoulder extending to about 3400 cm^{-1} from the main peak at 3250 cm^{-1} which has previously been described as a feature of crystalline ice.[37] This feature disappears as O atom irradiation proceeds indicating that the regularity of the crystalline hydrogen bond network is altered. Amorphisation of CSW has been observed previously when irradiating CSW with, for instance, protons[38] or photons.[18]

RAIR spectra reported in Fig. 5 through 7 followed equivalent O atom irradiation periods of 50 minutes consistent with formation of a 5 ML O_2 overlayer on the corresponding H_2O ice film. O_2 TPD measurements were then carried out on multilayer H_2O systems and the results of these TPD studies are summarised in Fig. 8. It is clear from Fig. 8 that the O_2 desorption profile changes in accord with the underlying 100 ML water film.

In Fig. 8(a), O_2 is adsorbed and reactively accreted on a porous and rough surface with reaction enthalpy release leading to isothermal compaction during O atom irradiation. Consequently, the O_2 TPD shows evidence of multilayer desorption (peaking at about 36.5 K) and monolayer desorption following at higher

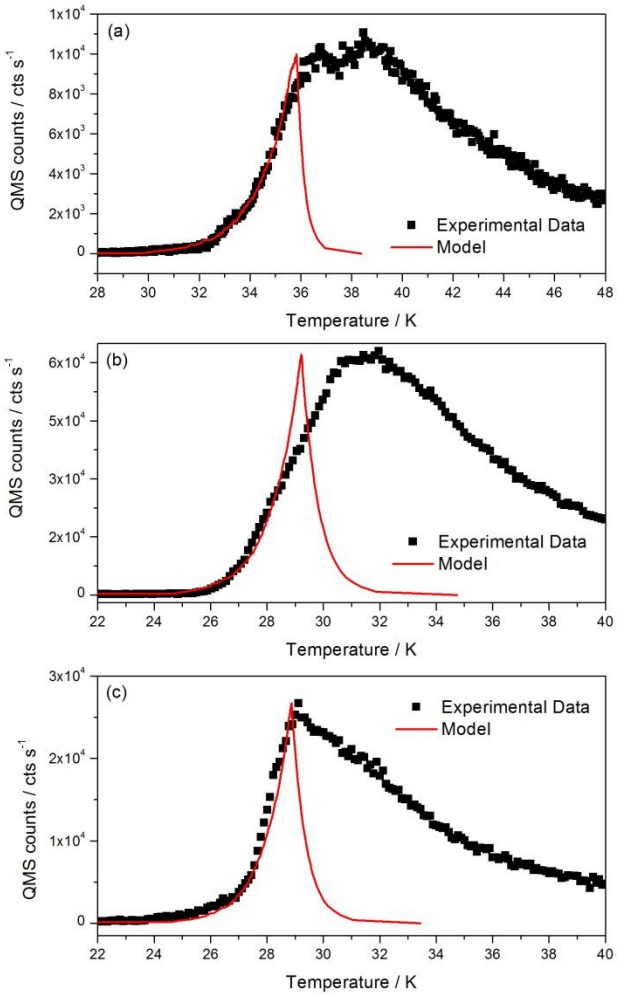

Fig. 8: TPD profiles of 5 ML (a) O_2 desorption from multilayer p-ASW, (b) O_2 desorption from c-ASW and (c) O_2 desorption from CSW. All O_2 films are deposited with the O:O_2 beam which promotes morphological change as described in the text. This clearly leads to changes in the E_{des} of O_2 multilayers but also potentially to trapping of O_2 in the H_2O matrix as in Collings *et al.*[39]

temperatures (peaking at about 38.5 K). The authors note that O_2 is detected at about 153 K as p-ASW crystallises to form CSW as well as O_2 co-desorbing with CSW. This is not inconsistent with our previous observations of CO.[39,40] The TPD of O_2 deposited and grown on c- ASW is shown in Fig. 8(b). c-ASW is known to show differences in surface reactivity and porosity[41,42] which results in differences in the multilayer O_2 peak desorption temperature (32 K) compared to the p-ASW film (36.5 K). During the c-ASW film experiments, O_2 was not detected as H_2O crystallises or desorbs at higher temperatures. Fig. 8(c) presents the O_2 desorption data for CSW. CSW has no pores and a less rough surface compared to the ASW films and so the TPD profile is more indicative of simple multilayer (and monolayer) desorption with the former peaking at about 29 K which is in line with previously mentioned data in Fig. 1 and multilayer desorption of O_2 from pure $aSiO_2$.[3] Fitting these data using the simple multilayer methodology above yields the additional E_{des} and ν parameters highlighted in Table 1. Of course, a more thorough analysis akin to that in our study of the trapping and

desorption of CO on p-ASW,[39,40] would yield relevant additional monolayer and trapped state parameters.

Conclusions and Astrophysical Implications

In summarising this work, we first highlight what we consider the key observations:

(1) H_2O de-wetting is observed as previously noted as happening on $aSiO_2$ and HOPG surfaces. While bombarding a sub-monolayer coverage of H_2O with O atoms, reaction enthalpy release as O_2 and O_3 formation enhances the H_2O agglomeration process. Further to this, reaction enthalpy release simultaneously promotes re-connection of the hydrogen-bonded network of porous H_2O agglomerates.

(2) Reaction enthalpy release is dissipated into the hydrogen-bonded network of a H_2O film promoting significant morphological changes of H_2O ice. From the presented results, compaction of p-ASW to c-ASW while CSW undergoes amorphisation to become more similar to c-ASW occurs as O_2 and O_3 are formed from an atomic oxygen beam.

(3) While the reaction enthalpy of O_2 formation leads to morphological changes, there is no evidence for reaction enthalpy promoted desorption of O_2 or H_2O hinting at efficient reaction energy dissipation into the underlayer. Further to this, atomic oxygen was not observed to desorb, outside of expected fragment patterns of O_2 and O_3, indicating full conversion of O to O_2 and O_3.

(4) Desorption of O_2 films from $aSiO_2$ have been shown to be highly dependent on deposition method. Background deposition compared to molecular beam deposition leads to a more open film due to differences in deposition rate, and hence adsorption enthalpy accommodation. This leads to higher desorption energies for molecular beam dosed O_2 as compared to background dosed. Comparing molecular and atomic beam dosing highlights further differences in desorption energy. Reaction enthalpy of O_2 formation is efficiently dissipated into the growing O_2 layer as well as the $aSiO_2$ substrate possibly leading to a more fractured film explaining the lower desorption energy compared to molecular beam dosed O_2.

In astrophysical environments O atom concentration with respect to H atom varies from around 3 to 10×10^{-8} molecules cm^{-2} in cold, dense objects.[43-46] Binary O-O reactions on grain surfaces are therefore likely to be few in number compared to O-H and H-H events. Reactive accretion of O-O is therefore a relatively minor channel compared to OH radical and H_2O molecule reactive accretion. Indeed, it is likely that O_2 is more readily formed on grains by energetic processing of solid H_2O as H_2 loss has been found to occur from solid H_2O irradiated with photons and charged particles.[47-49] However, our results suggest that when O_2 is formed, either directly by O-O recombination on the grain surface from incident atoms, or indeed through recombination of photolytically and radiolytically generated O atoms in solid H_2O, reaction enthalpy promoted desorption is unlikely to be significant. Rather our data suggest that the enthalpy release would enhance H_2O agglomeration rates (in the earliest phases on ice accumulation on grain surfaces); promote amorphisation of any crystalline ice clusters formed during the initial high temperature growth of ice in a low density environment; and encourage ice morphological change from p-ASW to c-ASW of ice is deposited in older, cold and dense environments.

We would go further to suggest that this is a general role for enthalpy release in many atom and radical recombination processes. Indeed, the work of Accolla *et al*.[15] suggests that this is not uncommon even for D_2 or H_2 formation where it is well-known that product D_2/H_2 is directly released into the gas phase carrying away some of the reaction enthalpy as internal energy.

The role of reaction enthalpy release in promoting H_2O agglomeration provides further support for the icy grain evolution model proposed by Rosu-Finsen *et al*.[9] on the basis of isothermal H_2O agglomeration experiments. It would seem likely therefore that icy grains will evolve in an environment favouring formation of H_2O islands on the grain surface and growth of ice from these islands by agglomeration of H_2O formed elsewhere on the grain surface and on the ice surface itself. This results in a grain that has regions of clean mineral or carbonaceous surface and regions of water ice surface onto which carbon monoxide might deposit as the density increases. With the James Webb Space Telescope about to be launched in 2018,[50] observations in interstellar environments with increasing density may provide the observational evidence to support this proposal.

Conflicts of interest

The authors declare no conflicts of interest.

Acknowledgements

The authors acknowledge the support of the UK Science and Technology Facilities Council (STFC, ST/M001075/1), the UK Engineering and Physical Science Research Council (EPSRC, EP/D506158/1) and the European Community FP7-ITN Marie-Curie Programme (LASSIE project, grant agreement #238258). ARF thanks HWU for a James Watt Scholarship.

References

1 A. G. G. M. Tielens, *Rev. Mod. Phys.*, 2013, **85**, 1021
2 M. Minissale, E. Congiu, and F. Dulieu, *J. Chem. Phys.*, 2014, **140**, 074705
3 M. P. Collings, V. L. Frankland, J. Lasne, D. Marchione, A. Rosu-Finsen, and M. R. S. McCoustra, *Mon. Not. R. Astron. Soc.*, 2015, **449**, 1826
4 H. M. Cuppen and E. Herbst, *Astrophys. J.*, 2007, **668**, 294
5 S. Ioppolo, H. M. Cuppen, C. Romanzin, E. F. van Dishoeck, and H. Linnartz, *Phys. Chem. Chem. Phys.*, 2010, **12**, 12065

6 H. M. Cuppen, S. Ioppolo, C. Romanzin, and H. Linnartz, *Phys. Chem. Chem. Phys.*, 2010, **12**, 12077
7 H. Mokrane, H. Chaabouni, M. Accolla, E. Congiu, F. Dulieu, M. Chehrouri, and J. L. Lemaire, *Astrophys. J. Lett.*, 2009, **705**, L195
8 E. F. van Dishoeck, E. Herbst, and D. A. Neufeld, *Chem. Rev.*, 2013, **113**, 9043
9 A. Rosu-Finsen, D. Marchione, T. L. Salter, J. W. Stubbing, W. A. Brown, and M. R. S. McCoustra, *Phys. Chem. Chem. Phys.*, 2016, **18**, 31930
10 D. Hollenbach, M. W. Werner, and E. E. Salpeter, *Astrophys. J.*, 1971, **163**, 165
11 E. Congiu, M. Minissale, S. Baouche, S. Cazaux, H. Chaabouni, G. Manico, A. Moudens, V. Pirronello, and F. Dulieu, *Faraday Discuss.*, 2014, **168**, 151
12 T. Lauck, L. Karssemeijer, K. Shulenberger, M. Rajappan, K. I. Oberg, and H. M. Cuppen, *Astrophys. J.*, 2015, **801**, 118
13 R. S. Smith, R. A. May, and B. D. Kay, *J. Phys. Chem. B*, 2016, **120**, 1979
14 S. Taj, D. Baird, A. Rosu-Finsen, and M. R. S. McCoustra, *Phys. Chem. Chem. Phys.*, 2017, **19**, 7990
15 M. Accolla, E. Congiu, F. Dulieu, G. Manicò, H. Chaabouni, E. Matar, H. Mokrane, J. L. Lemaire, and V. Pirronello, *Phys. Chem. Chem. Phys.*, 2011, **13**, 8037
16 J. P. Toennies, F. Traeger, J. Vogt, and H. Weiss, *J. Chem. Phys.*, 2004, **120**, 11347
17 G. A. Grieves and T. M. Orlando, *Surf. Sci.*, 2005, **593**, 180
18 G. Leto and G. A. Baratta, *Astron. Astrophys.*, 2003, **397**, 7
19 G. A. Kimmel, K. P. Stevenson, Z. Donhalek, R. S. Smith, and B. D. Kay, *J. Phys. Chem*., 2001, **114**, 5284,
20 G. A. Kimmel, K. P. Stevenson, Z. Donhalek, R. S. Smith, and B. D. Kay, *J. Phys. Chem*., 2001, **114**, 5295
21 H. J. Fraser, M. P. Collings, and M. R. S. McCoustra, *Rev. Sci. Instrum.*, 2002, **73**, 2161
22 V. L. Frankland, A. Rosu-Finsen, J. Lasne, M. P. Collings, and M. R. S. McCoustra, *Rev. Sci. Instrum.*, 2015, **86**, 055103
23 J. A. Noble, E. Congiu, F. Dulieu, and H. J. Fraser, *Mon. Not. R. Astron. Soc.*, 2012, **421**, 768
24 J. A. Noble, S. Diana, and F. Dulieu, *Mon. Not. R. Astron. Soc.*, 2015, **454**, 2636
25 M. P. Collings, M. A. Anderson, R. Chen, J. W. Dever, S. Viti, D. A. Williams, and M. R. S. McCoustra, *Mon. Not. R. Astron. Soc.*, 2004, **354**, 1133
26 A. Rosu-Finsen, Ph.D. Thesis, Heriot-Watt University, 2016, Icy dust grains in the interstellar medium: their properties and impact, link: www.ros.hw.ac.uk/handle/10399/3210
27 C. J. Bennett and R. I. Kaiser, *Astrophys. J.*, 2005, **635**, 1362
28 J. He, D. Jing, and G. Vidali, *Phys. Chem. Chem. Phys.*, 2014, **16**, 3493
29 B. Sivaramen, C. S. Jamieson, N. J. Mason, and R. I. Kaiser, *Astrophys. J.*, 2007, **669**, 1414
30 D. Jing, J. He, J.R. Brucato, G. Vidali, L. Tozzetti, and A. De Sio, *Astrophys J.*, 2012, **756**, 98
31 J. T. Herron and H. I. Schiff, *J. Chem. Phys.*, 1956, **24**, 1266
32 R. Atkinson, D. L. Baulch, R. A. Cox, J. N. Crowley, R. F. Hampson, R. G. Hynes, M. R. Jenkin, M. J. Rossi, and J. Troe, *Atmos. Chem. Phys.*, 2014, **4**, 1461
33 H. E. Avery and D. J. Shaw, *Basic Physical Chemistry Calculations, 2nd Edition* (Butterworth–Heinemann Ltd., Oxford, 1980)
34 P. Ehrenfreund, P. A. Gerakines, W. A. Schutte, M. C. van Hemert, and E. F. van Dischoeck, *Astron. Astrophys.*, 1996, **312**, 263
35 S. S. Xantheas and T. H. Dunning Jr., *J. Chem. Phys.*, 1993, **99**, 8774
36 J. D. Thrower, M. P. Collings, F. J. M. Rutten, and M. R. S. McCoustra, *Mon. Not. Roy. Astron. Soc.*, 2009, **394**, 1510
37 A. S. Bolina, A. J. Wolff and W. A. Brown, *J. Phys. Chem. B*, 2005, **109**, 16836
38 M. H. Moore and R. L. Hudson, *Astrophys. J.*, 1992, **401**, 353
39 M. P. Collings, J. W. Dever, H. J. Fraser, M. R. S. McCoustra, and D. A. Williams, *Astrophys. J.*, 2003, **583**, 1058
40 M. P. Collings, J. W. Dever, H. J. Fraser, and M. R. S. McCoustra, *Astrophys. Space Sci.*, 2003, **285**, 633
41 J. E. Schaff and J. T. Roberts, *J. Phys. Chem.*, 1996, **100**, 14151
42 J. E. Schaff and J. T. Roberts, *Langmuir*, 1999, **15**, 7232
43 P. F. Goldsmith, G. J. Melnick, E. A. Bergin, J. E. Howe, R. L. Snell, D. A. Neufeld, M. Harwit, M. L. N. Ashby, B. M. Patten, S. C. Kleiner, R. Plume, J. R. Stauffer, V. Tolls, Z. Wang, Y. F. Zhang, N. R. Erickson, D. G. Koch, R. Schieder, G. Winnewisser, and G. Chin, *Astrophys. J.*, 2000, **539**, L123
44 B. Larsson, R. Liseau, L. Pagani, P. Bergman, P. Bernath, N. Biver, J. H. Black, R. S. Booth, V. Buat, J. Crovisier, C. L. Curry, M. Dahlgren, P. J. Encrenaz, E. Falgarone, P. A. Feldman, M. Fich, H. G. Florén, M. Fredrixon, U. Frisk, G. F. Gahm, M. Gerin, M. Hagström, J. Harju, T. Hasegawa, Å. Hjalmarson, L. E. B. Johansson, K. Justtanont, A. Klotz, E. Kyrölä, S. Kwok, A. Lecacheux, T. Liljeström, E. J. Llewellyn, S. Lundin, G. Mégie, G. F. Mitchell, D. Murtagh, L. H. Nordh, L.-Å. Nyman, M. Olberg, A. O. H. Olofsson, G. Olofsson, H. Olofsson, G. Persson, R. Plume, H. Rickman, I. Ristorcelli, G. Rydbeck, A. A. Sandqvist, F. V. Schéele, G. Serra, S. Torchinsky, N. F. Tothill, K. Volk, T. Wiklind, C. D. Wilson, A. Winnberg, and G. Witt, *Astron. Astrophys.*, 2007, **466**, 999
45 A. A. Sandqvist, B. Larsson, A. Hjalmarson, P. Bergman, P. Bernath, U. Frisk, M. Olberg, L. Pagani, and L. M. Ziurys, 2008, *Astron. Astrophys.*, 482, 849
46 R. Liseau, P. F. Goldsmith, B. Larsson, L. Pagani, P. Bergman, J. Le Bourlot, T. A. Bell, A. O. Benz, E. A. Bergin, P. Bjerkeli, J. H. Black, S. Bruderer, P. Caselli, E. Caux, J.–H. Chen, M. de Luca, P. Encrenaz, E. Falgarone, M. Gerin, J. R. Goicoechea, Aa. Hjalmarson, D. J. Hollenbach, K. Justtanont, M. J. Kaufman, F. Le Petit, D. Li, D. C. Lis, G. J. Melnick, Z. Nagy, A. O. H. Olofsson, G. Olofsson, E. Roueff, Aa. Sandqvist, R. L. Snell, F. F. S. van der Tak, E. F. van Dishoeck, C. Vastel, S. Viti, and U. A. Yildiz, *Astron. Astrophys.*, 2012, **541**, A73
47 W. Zheng, D. Jewitt, and R. I. Kaiser, *Astrophys. J.*, 2006, **639**, 534
48 N. G. Petrik and G. A. Kimmel, *Phys. Rev. Lett.*, 2003, **90**, 166102
49 A. G. M. Abdulgalil, A. Rosu-Finsen, D. Marchione, J. D. Thrower, M. P. Collings, and M. R. S. McCoustra, *ACS Earth and Space Chem.*, 2017, **1**, 209
50 Link to website: https://jwst.nasa.gov/whatsNext.html

